Magneto-hydro-dynamic limits in spherical tokamaks

T. C. Hender, S. J. Allfrey, R. Akers, L. C. Appel, M. K. Bevir et al.

Citation: Phys. Plasmas **6**, 1958 (1999); doi: 10.1063/1.873493
View online: http://dx.doi.org/10.1063/1.873493
View Table of Contents: http://pop.aip.org/resource/1/PHPAEN/v6/i5
Published by the American Institute of Physics.

Magneto-hydro-dynamic limits in spherical tokamaks*

T. C. Hender,† S. J. Allfrey, R. Akers, L. C. Appel, M. K. Bevir, R. J. Buttery, M. Gryaznevich, I. Jenkins, O. J. Kwon,[a] K. G. McClements, R. Martin, S. Medvedev,[b] M. P. S. Nightingale, C. Ribeiro, C. M. Roach, D. C. Robinson, S. E. Sharapov,[c] A. Sykes, L. Villard,[d] and M. J. Walsh
Euratom/UKAEA Fusion Association, Culham Science Centre, Abingdon, Oxon OX14 3DB, United Kingdom

(Received 16 November 1998; accepted 22 January 1999)

The operational limits observed in spherical tokamaks, notably the small tight aspect ratio tokamak (START) device [A. Sykes *et al.*, Nucl. Fusion **32**, 694 (1992)], are consistent with those found in conventional aspect ratio tokamaks. In particular the highest β achieved ($\sim$40%) is consistent with an ideal magneto-hydro-dynamic (MHD) Troyon type limit, the upper limit on density is well described by the Greenwald density ($\pi a^2 \overline{n_e}/I_p \sim 1$) and the normalized current (I_p/aB_t) is limited such that $q_{95} \gtrsim 2$. Stability calculations indicate scope for increasing both normalized β and normalized current beyond the values so far achieved, although wall stabilization is generally needed for low-n modes. In double null configurations current terminating disruptions occur at each of the operational boundaries, though the current quench tends to be slow at the density limit and disruptions at high β may be due to the low q. In early limiter START discharges, before the divertor coils were installed, disruptions rarely occurred. Instead internal reconnection events which have all the characteristics of a disruption except the current quench occurred. These various disruptive behaviors are explained in terms of a model in which helicity is conserved during the disruption. Due to the low toroidal field beam ions in START, and α particles in a ST power plant, are super-Alfvénic. This gives the possibility for toroidal Alfvén eigenmodes (TAEs) to occur and such modes are frequently observed in START neutral beam injection (NBI) discharges, but seem to be benign. The features of these observed TAEs are shown to be in agreement with MHD calculations. © *1999 American Institute of Physics.* [S1070-664X(99)95005-X]

I. INTRODUCTION

The primary original motivation for the tight aspect ratio or spherical tokamak (ST) was its predicted high β limit.[1] The basis of this prediction is the Troyon[2] or Sykes–Wesson[3] ideal magneto-hydro-dynamic (MHD) β limit, which can be written in the form:

$$\beta < \frac{C\epsilon(1+\kappa^2)}{q_*} \tag{1}$$

where $q_* = aB_\phi/(RB_\theta)(1+\kappa^2)/2$, $\kappa = b/a$ is the plasma elongation, $\epsilon = a/R$ is the inverse aspect ratio, and C is a constant. Since by definition ϵ is maximized in the ST and high natural elongation is possible,[1] Eq. (1) demonstrates the possibility of high β in the ST. However rather than exploring the β limit the initial MHD role of the small tight aspect ratio tokamak (START) device[4] at Culham was more to test the general MHD properties of the ST—the relatively large poloidal field in the ST means that in some respects it lies between the conventional tokamak, the spheromak, and the pinch, and there was the possibility that the MHD behavior could be pinch-like with an undesirable impact on energy confinement. In fact operation of START, and other STs worldwide [e.g., the current drive experiment-upgrade[5] (CDX-U), the helicity injected tokamak[6] (HIT), the Madison educational small aspect ratio tokamak[7] (MEDUSA), and the Tokyo spherical tokamak[8] (TST-M)], has shown that MHD activity in the ST is very similar to the conventional aspect ratio tokamaks—with one significant exception that disruptions and their consequences can be less severe.

The initial success of the START ST led to the installation of neutral beam injection (NBI) heating, which has now allowed the original limit predictions of high β to be verified.[9,10] NBI has also created a super-Alfvénic population of fast ions, allowing the study of Alfvén resonance MHD, such a toroidal Alfvén eigenmodes (TAEs). Further NBI heating has extended the operating domain, confirming previous Ohmic results,[11] that the plasma density is bounded by a normalized Greenwald density,[12] $\pi a^2 \overline{n_e}/I_p \sim 1$. Operationally there is an empirical limit $q_{95} \gtrsim 2$, though MHD stability calculations indicate that the normalized plasma current may be increased beyond this limit.

This paper deals with the MHD associated with the various performance limits discussed above. Since much of the data in this paper comes from the START machine, a brief description of its main features is given in the next section. Then in Sec. III the MHD phenomena which limit high β and low-q discharges are covered. Also in this section the prospects for MHD stable operation at still higher β are examined. The MHD phenomena associated with the density

*Paper B1I1.6 Bull. Am. Phys. Soc. **43**, 1637 (1998).
†Invited speaker.
[a]Taegu University, Taegu, Republic of Korea.
[b]Keldysh Institute, Moscow, Russia.
[c]JET Joint Undertaking, Abingdon, UK.
[d]CRPP, Euratom-Confédëration Suisse, EPFL, Lausanne, Switzerland.

limit are discussed in Sec. IV and some initial results using pellet injection to exceed the density limit are also described. Discharges at high β and/or low-q suffer from current terminating disruptions in the present START double null configuration. In general disruptivity increased in START with the introduction of divertor coils; the reasons underlying this are examined in Sec. V. When a disruption occurs then the double null START plasmas can be vertically unstable but even then the measured halo currents on the center column are modest—this issue is also discussed in Sec. V. Turning to the much higher frequency MHD, driven by the fast NBI ions, results on TAEs and fishbone-like[13,14] oscillations are discussed in Sec. VI. Finally conclusions are drawn in Sec. VII.

II. START PARAMETERS

Typical START plasmas in the post-October 1996 double null divertor configuration had major radii ~0.3–0.4 m, minor radii in the range 0.2–0.3 m, aspect ratio in the range 1.25–1.5 and elongation ~1.7. The plasma current was in the range 100–300 kA with toroidal field 0.15–0.4 T, the field being ramped down to attain the highest β. The NBI heating provided up to 800 kW of absorbed power with the 30 keV hydrogen beam coinjected into a deuterium target plasma. The beam line was approximately tangential to the magnetic axis.

The primary MHD diagnostics on START are the Mirnov coils. There is a set of 46 coils, at different heights on the center column, measuring dB_Z/dt; these coils are in toroidally opposite pairs at each height, allowing even and odd-n combinations to be formed (n being the toroidal mode number). Since plasmas in START can be formed by a compression technique,[4] this limits the scope for outboard magnetic fluctuation measurements, though in some cases a coil on a movable midplane probe assembly is available ~2 cm from the outboard plasma boundary. In addition for analyzing MHD behavior vertical and horizontal soft x-ray (SXR) arrays exist. There are also the standard equilibrium magnetic diagnostics, an interferometer to measure density, and a multipoint single time Thomson scattering system. All the equilibrium data are used as constraints to the EFIT equilibrium code,[15] which is the primary vehicle for calculating equilibrium properties (e.g., β) on START.

There is also a dedicated coil set for measuring halo currents on the center column. This consists of six partial Rogowskii coils, to determine toroidal asymmetries, at $Z = 0.63$ m, which is ~15 cm above the divertor X-point height.

III. HIGH-β MHD LIMITS, EDGE-q LIMITS AND FUTURE PROSPECTS

A. Experimental observations and analysis

START has fulfilled early theoretical expectations[1] by achieving high β. In particular a toroidal $\beta_t \sim 40\%$ has been achieved,[16] where $\beta_t \equiv 2\mu_0 \langle P \rangle / B_0^2$ with angled brackets denoting volume averages and B_0 being the vacuum toroidal magnetic field at the plasma geometric axis. Furthermore,

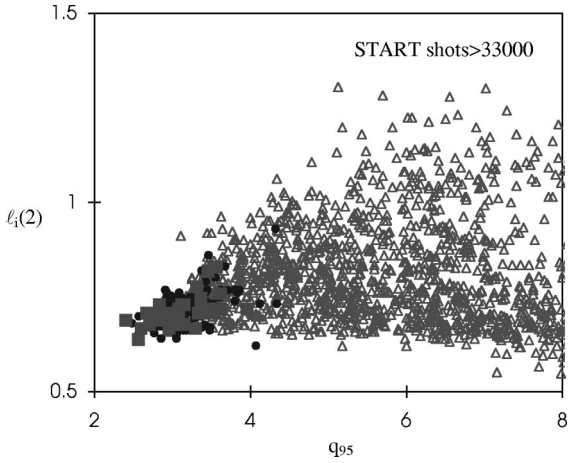

FIG. 1. Operational domain for START with solid squares representing pulses with $\beta_t > 30\%$, solid circles $\beta_t > 20\%$, and open triangles $\beta_t < 20\%$.

since the fast ion contribution to the pressure from the beams is rather centrally peaked a central $\beta_0 = 2\mu_0 P_0 / B_{\mathrm{mag}}^2 \sim 150\%$ has been achieved,[16] where P_0 and B_{mag} are the pressure and vacuum toroidal field at the magnetic axis. High β is achieved in START by ramping down the toroidal field; this necessarily means that high-β pulses have low-q ($q_{95} \leqslant 3$ to 4)—this is shown in Fig. 1 where the operational domain for START in the $l_i(2)$-q_{95} plane is plotted, with pulses with $\beta_t > 30\%$ and 20% highlighted; here $l_i(2) = \int B_p^2 dv / (B_{\mathrm{pa}}^2 V)$ with B_{pa} the average poloidal field at the boundary. Note that Fig. 1 shows an empirical operation limit in START of $q_{95} \lesssim 2$.

All START high-β pulses terminate in a disruption, an example for one of the highest-β pulses is shown in Fig. 2. From this figure it can be seen that there is a distinct energy quench phase before the current quench, in line with observations in conventional tokamaks.[17] The duration of the energy quench is found to be consistent with expectations from conventional tokamak databases.[18] During this energy quench phase visible light emission from the divertor leg which is in the electron ∇B-direction is observed, this seems to be associated with enhanced losses but the exact cause is not understood.

Apart from regular sawteeth ($\tau_{\mathrm{saw}} \sim 1.5$ ms) the high-β discharges show little coherent MHD until the disruption. During the energy quench there is generally a coherent 60–120 kHz mode (see Fig. 3); the strength of this mode correlates well with the degree of energy quench. This mode is odd-n, probably $n = 3$ or 5 from its frequency. The spectrogram (Fig. 3) also shows a zero frequency feature, which is coincident with the initiation of the energy quench. This feature is even-n but because of the limited magnetic diagnostics it is not possible to determine if this is due to an axisymmetric equilibrium change ($n = 0$) or a locked mode (presumably $n = 2$). The MHD behavior which is observed during the energy quench is internal (in general there are no visible distortions to the plasma boundary) and not characteristic of ideal β-limit modes.

Stability calculations for these high-β pulses are compli-

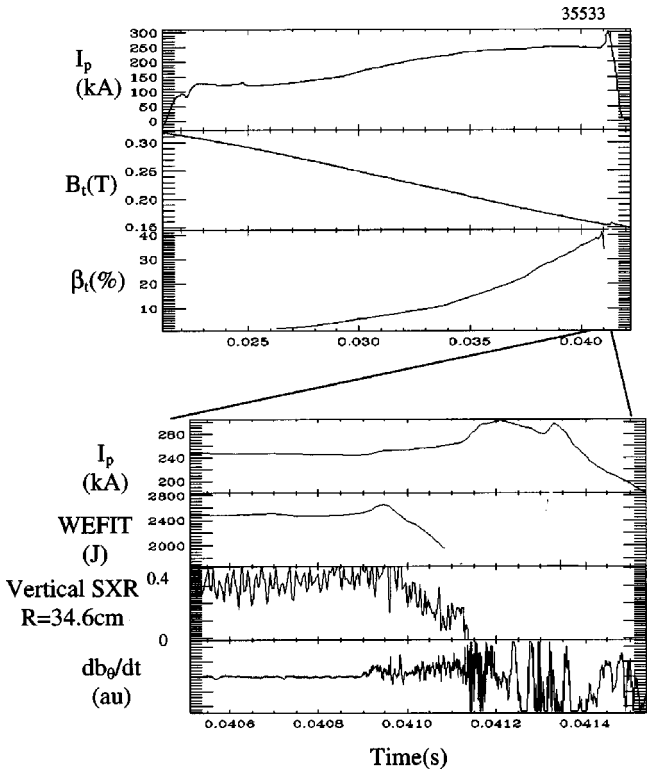

FIG. 2. Record β START pulse. The lower traces show an expanded time near the disruption. The bottom signal is from an inboard Mirnov probe located in the center column at the midplane.

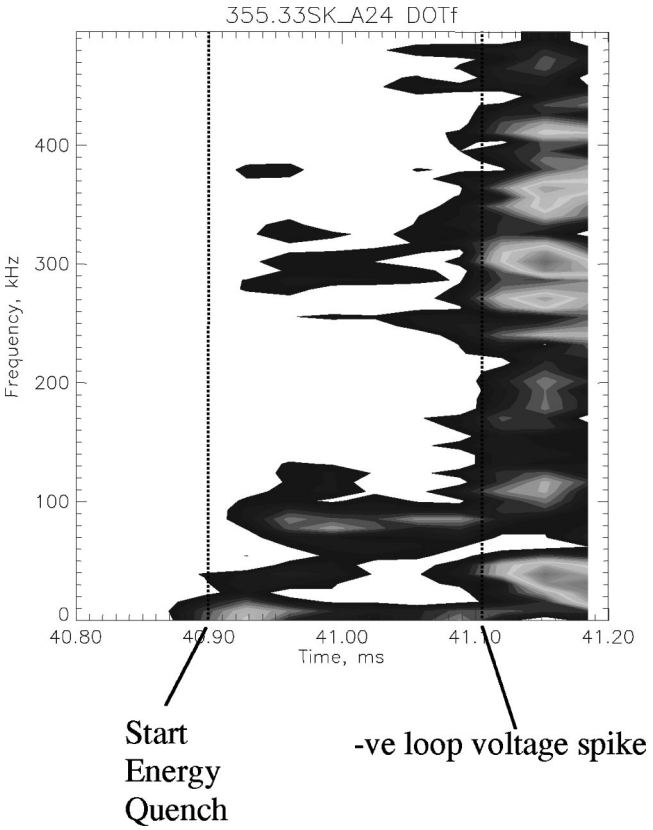

FIG. 3. Spectrogram during disruption for midplane inboard Mirnov probe for same high-β pulse as Fig. 2. Lightest shades are high intensity signals. Lines denote times when energy and current quench begin.

cated by the fact that there is a moderate fast particle content ($W_{\text{fast}}/W \sim 20\%$) from the NBI. However to make an initial assessment of the consistency of the experimental results with ideal MHD expectations, codes which do not treat fast particle effects on equilibrium or stability are used. The equilibria are obtained from EFIT[15] using the kinetic measured pressure profile combined with the calculated fast particle pressure profile. The stability of these cases has been calculated using the CAXE and KINX[19] equilibrium and stability codes, which include the full separatrix geometry in the stability calculation. Figure 4 shows the ballooning, $n=1$, 2, 3, and 4 stability limits for pulse 36 544. For the calculations presented in this figure the q profile is fixed while the pressure profile is varied to determine stability limits. Optimizing the pressure profile to give marginal ballooning stability on every surface gives $\beta_t = 39\%$, which is close to the highest β achieved experimentally in this pulse. Since $q_0 = 0.85$ is assumed for these EFIT equilibria, consistent with the occurrence of sawteeth and the observed sawtooth inversion radius, the marginal ballooning pressure profile is very flat within $q=1$; this is similar to the measured thermal pressure profile but the fast particle pressure is strongly peaked within $q \sim 1$.[16] The $n=1$ mode (no wall), keeping the same pressure profile shape as the marginal ballooning case [which has $P'(q=1)/P'(\max)=0.2$], is marginally stable at the ballooning β limit ($\beta_t = 39\%$). There is strong sensitivity to the pressure gradient within $q=1$ due to coupling between the $m=1$ internal kink and the external kink—the low-n stability limits shown in Fig. 4, use a pressure profile with $P'(q=1)/P'(\max)=0.015$ (which is marginally ballooning stable at $\beta_t = 37\%$), giving $n=1$ to 4 β_t limits above the experimental value. Further reducing the pressure gradient within $q=1$ [$P'(q=1)/P'(\max)=10^{-6}$] leads to an $n=1$ limit (no wall) of $\beta_t = 63\%$. The magnetic shear within $q=1$ also affects the β limit, if there is a finite pressure gradient for $q<1$, by changing the internal kink stability. Although there is uncertainty arising from the pressure gradient and magnetic shear within $q=1$, the observation that discharges at low β which are otherwise equivalent to the highest-β pulses (notably in q_{95}) also disrupt suggests that is not low-n β-driven modes which are causing the disruption. It is likely that it is a q_{95} limit and not a β limit which is limiting the achievable

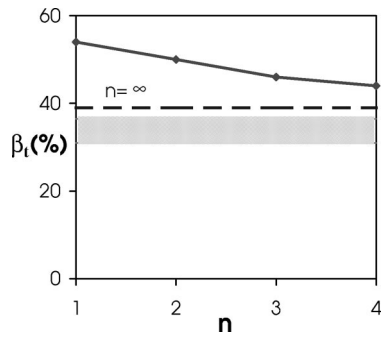

FIG. 4. Ideal low-n (no wall) and ballooning stability limits ($n=\infty$) for START pulse 36544. The shaded region represents the range of β_t predicted by EFIT allowing for uncertainties in plasma edge current and Z_{eff} (1.5–2.5 in calculation of the fast ion pressure).

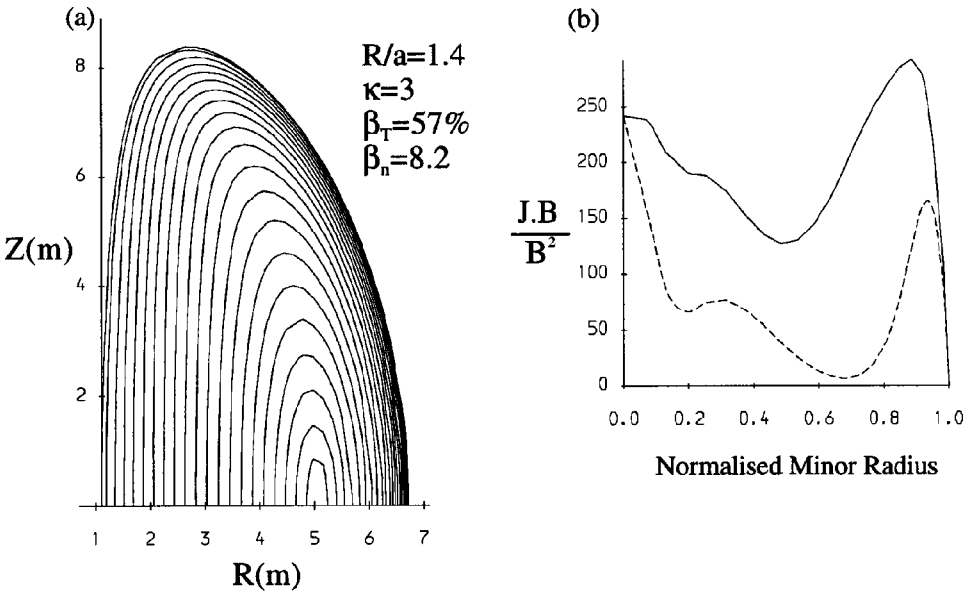

FIG. 5. (a) Flux surfaces for second ballooning mode stable case; (b) flux surface averaged current profile (solid line) and required external current drive (broken line).

β; in effect the achievable β is limited by the available NBI power which is in accord with the increase in β achieved each time the NBI power has been incremented on START.

B. Theoretical calculations on future prospects for higher β

It is interesting to examine from a MHD stability viewpoint the prospects for further increases in β; such increases are desirable for economic reasons in power plant designs.[20] Current profile optimization is one obvious route to explore. On conventional aspect ratio tokamaks it is known that the normalized $\beta_n \sim 4l_i$.[21] This route for optimizing β, by ramping down I_p to increase l_i, has been tested on START; this did not lead to higher β_n however because operational limits mean higher l_i can only be achieved at higher q_{95}, and thus higher B_t, and in this regime performance is limited by the available power.

Taking the profile optimization a step further, theoretical calculations suggest yet higher β_n can be achieved in the second ballooning stable regime. An example of a second-ballooning-stable case is shown in Fig. 5 with $R/a=1.4$, $\beta_n=8.2$, $\beta_t=57\%$, $\langle\beta\rangle=2\mu_0\langle P\rangle/\langle B^2\rangle=41\%$ and a toroidal pressure driven current fraction (bootstrap+diamagnetic) of 88%. This case is attractive from the viewpoint of a steady-state power plant design because the high pressure driven current fraction lowers the need for expensive external current drive; it is found from detailed Monte Carlo current drive calculations that, for an $I_p=31$ MA power plant design, the residual current density profile (total of 4.4 MA) can be driven with 74 MW of NBI. The penalty for improved ballooning mode stability is that an ideal wall is needed to stabilize low-n modes. For $n=1$ and $n=2$, the equilibrium shown in Fig. 5 requires a wall at $\sim$1.2 minor radii. The low-n stability here has been calculated with the MISHKA code[22] and verified by the KINX code (run with a limited plasma), and is very much in accord with calculations from other groups.[23,24]

The alternative route to increasing β is to increase the normalized current $I_n \equiv I\,(\mathrm{MA})/a(m)B_0(T)$. Calculations with the KINX code, including the full separatrix geometry in the stability calculations, indicate that there is scope for raising I_n; initially considering a sequence of equilibria with $\beta=0$ and a prescribed current profile $I^*=dJ/ds=(1-\Psi)^\alpha$ demonstrates normalized currents up to $I_n=16$ and 31 can be achieved at $R/a=1.35$ and 1.1, respectively, as shown in Fig. 6 (where dJ/ds is the derivative with respect to flux surface area of the current within the flux surface). These results should be contrasted with the maximum normalized current achieved in START of $I_n=8.2$ at $R/a=1.39$. Ballooning stability calculations for these cases show the expected limit of $\beta_n \sim 4.0$–4.5, which implies that very high β_t (>150% at $R/a=1.1$) can be achieved. Such high β values do require wall stabilization for low-n modes, for example at $R/a=1.35$ a ballooning stable case with $\beta_t \sim 65\%$ ($\beta_n=4.1$) requires a conformal wall at 1.3 minor radii. However, by reducing I_n somewhat from its $\beta=0$ limit, it is possible to achieve low-n stability with no wall; Fig. 7 shows the profiles for such a case with $\beta_t=107\%$, $I_n=24.1$, and $R/a=1.1$.

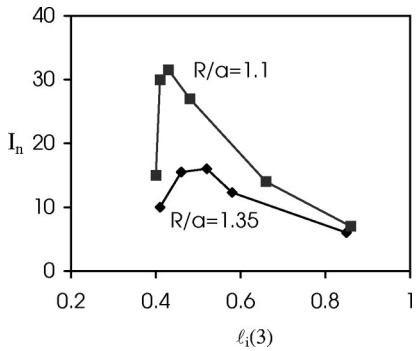

FIG. 6. Normalized current limit with no wall for $R/a=1.1$ and 1.35. The boundary shape is that of START ($\kappa=1.8$). Here $l_i(3)=2\int B_p^2\,dv/(R_0I^2)$. At the highest I_n for both aspects ratios $l_i(3)\sim 0.5$.

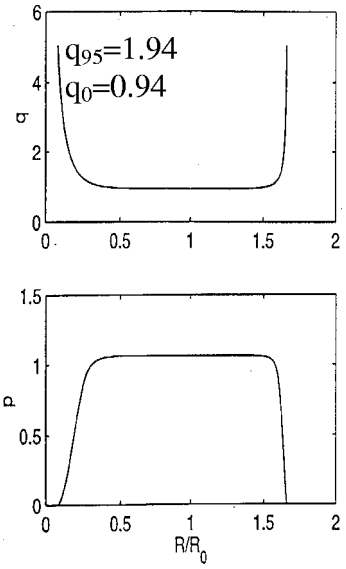

FIG. 7. High normalized current case ($R/a=1.1$) which is stable to low-n modes with no wall.

Three points should be noted about these high normalized current cases. First, they are very low β_p ($=0.071$ for the case in Fig. 7) and hence they are very strongly paramagnetic which means the volume average β is much lower. Second, the low β_p also gives a low bootstrap fraction ($\sim$10%) probably making such cases less attractive as the basis for a power plant, because of the need for a large amount of external current drive and third, these results can only be obtained when the full separatrix geometry is taken into account in the stability calculations; truncating the boundary results in low edge-q equilibria which are always unstable even at $\beta=0$, as demonstrated in previous fixed boundary calculations.[25]

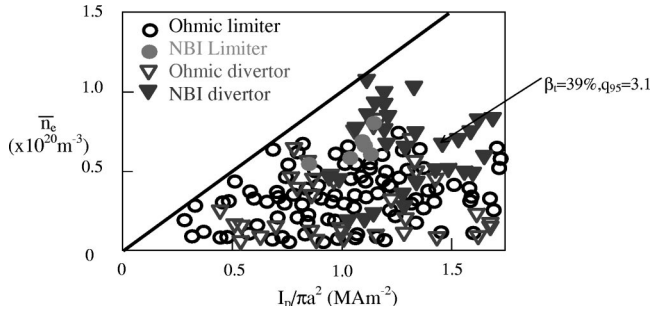

FIG. 8. Density limit operating space for START, showing operation domain is described well by the Greenwald density, $n_{GW}=1$ (solid line).

IV. DENSITY LIMIT OPERATING SPACE

The operating space of START is well defined by the Greenwald density, $n_{GW}\sim 1$, where $n_{GW}=\pi a^2 n_e / I_p[10^{20}\,\mathrm{m}^{-1}\,\mathrm{MA}^{-1}]$, as shown in Fig. 8. The density limit in limiter operation tends to be a soft limit with a sequence of internal reconnection events (IREs) limiting the density [Fig. 9(b)]. For diverted discharges increasingly hard disruptions [Fig. 9(a)] occur as $n_{GW}\sim 1$ is approached, although the current quench times ($\sim$1 ms from peak current to 10%) are longer than at high β and/or low q. Possible reasons for the differing behavior in limiter and double null configurations are discussed in Sec. V. There is no clear evidence, in general, for a rotating low m,n precursor to these density limit events, although the absence of outboard magnetic fluctuation measurements may mean that precursors are not being observed.

A pellet injector installed on START has allowed the density limit operating space to be extended. This was used to inject a single pellet of frozen deuterium, launching from the top/inboard side; the pellet ablates and can fuel the

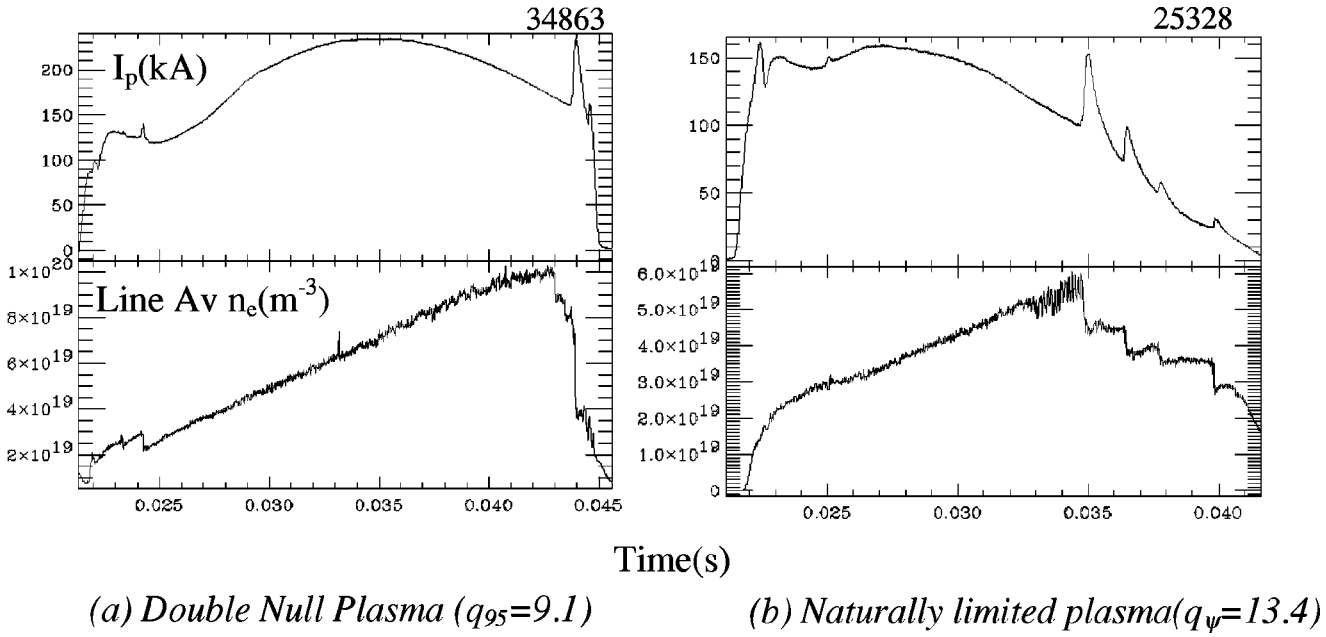

FIG. 9. Two discharges with a maximum $n_G(=\pi a^2 n_e/I_p)\sim 0.91$. Note the second smaller reconnection in the double null diverted case which gives rise to a longer overall current quench time.

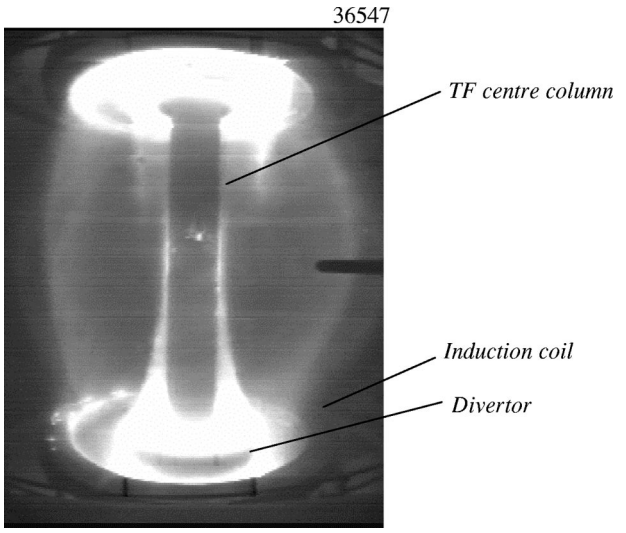

FIG. 10. Shows strong plasma elongation which occurs during the disruption, causing material interaction with the divertor coil. The black shadow on the RHS midplane is a movable probe (outside the plasma).

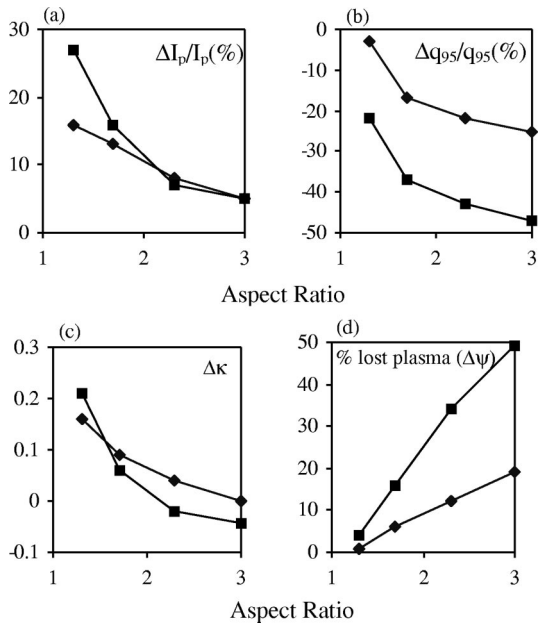

FIG. 11. Effect of IRE ($\Delta l_i = -0.3$) at various aspect ratios, with plasma elongation at its natural value (i.e., a uniform vertical field). The lines marked with squares have total thermal energy loss, while those with diamonds have a 50% loss. Here (a) is percentage increase in I_p, (b) the percentage decrease in edge-q, (c) the change in elongation, due to the IRE, and (d) the fraction of lost plasma measured by the reduction in poloidal flux inside the limiter flux surface.

plasma close to the center. Results show increases in plasma density of up to a factor three, and extend the operating space, approaching a Greenwald number $n_{GW} \sim 1.5$ and Murakami parameter $M = \overline{n}_e R/B(10^{20}\,\mathrm{m}^{-2}\,\mathrm{T}) \sim 2.4$.[26]

V. DISRUPTIONS AND VDEs

A. Experimental observations

Early operation in START,[27] as in several other STs (e.g., CDX-U[28]), showed the configuration was resilient to disruptions. In START operation almost no rapid current terminating disruptions were observed pre-October 1995 (the main exceptions being cases with a rapid vertical field ramp where the plasma is forced to interact strongly with the center post). However, as discussed above, more recent operation, most notably in the high-I_n regime, has led to rapid current-terminating disruptions. In fact the likelihood of disruptions in START is closely related to the machine configuration—in October 1995 divertor coils were installed and these were subsequently moved closer to the plasma (from $Z = \pm 0.54$ to 0.49 m) in December 1996. Both of these configuration changes resulted in an increased disruption frequency (it should be noted that, being a small tokamak, no particular attention is paid to avoiding disruptions during current rampdown in START). The dependence on configuration suggests that disruptions may be being caused by plasma interactions with the divertor coils—this is supported by visible light charge coupled device (CCD) images that show a strong plasma elongation and interaction with the divertor coils at the time of the disruption (Fig. 10).

Prior to October 1995 START had events, termed internal reconnections events, which had all the signatures of a disruption except that rapid current termination did not occur. During an IRE energy was lost (typically ~30%–40%) and a current spike (typically $\Delta I_p/I_p \sim 10\% - 15\%$) occurred (along with the associated negative loop voltage spike) but the current did not rapidly terminate. Normally the current returned to its pre IRE evolution, as if the IRE had not occurred [as shown in Fig. 9(b)].

B. Theory model

A model was developed to aid understanding of these IREs. Detailed Thomson scattering measurements, of the plasma electron temperature and density during an IRE, were used along with magnetic measurements to make pre- and post-IRE equilibrium reconstructions. The conservation of various quantities (e.g., magnetic energy, poloidal flux, plasma helicity) during the IRE was tested against these equilibria. It was found that plasma helicity was the most nearly conserved quantity, when the voltages applied to the moving plasma boundary by the changing poloidal and toroidal flux linked by the plasma (ψ,ϕ) are taken into account, so that the helicities in the initial and final states (subscripts i and f) are related by $dK/dt = -2\phi d\Psi/dt$ which in numerical form is

$$K_f - K_i = -(\phi_f + \phi_i)(\psi_f - \psi_i), \tag{2}$$

with helicity defined as $K = \int \mathbf{A}\cdot\mathbf{B}dV - \phi\psi$. This observation allows the effects of IREs to be modeled. Starting from a specified initial (''pre-IRE'') state an IRE is associated with a prescribed reduction in β_p and l_i, leading to a final state in which helicity is conserved according to Eq. (2). In this modeling the functional forms chosen for the plasma current density and pressure account for the observed flattening during the IRE. This IRE model has been applied to a range of aspect ratios, with natural elongation plasmas, giving the results shown in Fig. 11. It can be seen from Fig. 11(c) that a

much higher increase in elongation occurs at low aspect ratio; this has the effect of minimizing the change in edge-q [Fig. 1(b)], which will be beneficial since it keeps the post-IRE plasma farther from the kink mode limits at low q. Also from Fig. 11(d) it can be seen that there is substantially less loss of plasma at low aspect ratio; this result assumes the edge of the plasma undergoes force free motion which is the weighted average of attempts to follow the poloidal and toroidal flux resulting in plasma loss due to limiter interaction. So it is thought to be the small changes in edge-q and modest plasma loss which prevent the IRE turning into a full current terminating disruption at low aspect ratio. This model assumes an inboard limiter but allows uninhibited vertical elongation of the plasma. If the post-October 1995 START diverted plasma is modeled assuming helicity conservation during an IRE (Fig. 12), then strong interaction occurs with the divertor coils (as seen experimentally, Fig. 10) presumably resulting in a large impurity influx and hence the much greater likelihood of disruptions in double null START plasmas.

Intrinsically high natural elongations occur at tight aspect ratio[1] and it has been experimentally demonstrated in START[29] that elongations of ~ 3 can be obtained at low l_i. However, it is possible in the diverted START configuration to elongate the plasma beyond its natural elongation, so that a vertical displacement event (VDE) occurs following a disruption. In conventional aspect ratio tokamaks a serious consequence of a VDE is that substantial halo currents ($\sim 50\%$ of the predisruption I_p) can flow into parts of the vessel structure around the plasma and that these can be strongly toroidally asymmetric. If such asymmetric halo currents were to flow into the center post of a tight aspect ratio device, this could have serious design implications for future technology applications. However, measurements on START and CDX-U[28] indicate modest halo currents. The START measurements are made using the dedicated coils described in Sec. II and show toroidally averaged halo currents in the center post, $I_{\mathrm{halo}}/I_p(0) < 3\%$, with typically a toroidal peaking factor <1.3. This result is promising but needs to be more fully explored, with a more extensive set of halo current diagnostics, in the next generation of STs.

VI. FAST ION DRIVEN MHD

With the hydrogen beam injection used in START, the majority of beam protons were born with energies $E \sim 30\,\mathrm{keV}$ and hence speeds of about $2.4\times 10^6\,\mathrm{ms}^{-1}$, while the Alfvén velocity $\sim 10^6\,\mathrm{ms}^{-1}$. Fusion α particles ($E \sim 3.5\,\mathrm{MeV}$) in an ignited ST plasma would also be born with speeds in excess of the Alfvén velocity and so the possible excitation of Alfvénic instabilities, with the potential of some ensuing performance degradation, is an issue for ST power plants (though orbit squeezing due to high poloidal fields is thought to mitigate any effects). The introduction of beam ions into START thus provides an opportunity to investigate processes which are likely to be important for plasma performance in tokamak power plants generally, and ST power plants in particular.

In the majority of beam-heated START discharges, high frequency MHD magnetic fluctuations were observed. These fell into several distinct categories: brief descriptions of these are given below for modes up to 500 kHz.

A. Chirping modes and fishbones

In moderate and high β shots the most common type of high frequency instability occurred in the frequency range 50–350 kHz, the mean frequency sweeping down by a factor of two or so in a time of order 0.1–0.2 ms, as shown in Fig. 13 (28–34 ms). We refer to such bursts as chirping modes: a similar phenomenon has been observed on DIII–D.[30] These modes disappear when the electron density $\bar{n}_e > 10^{20}\,\mathrm{m}^{-3}$. The dominant toroidal component of these chirping bursts is generally $n = \mathrm{odd}$ (probably $n=1$). They do not appear to be affected significantly by sawteeth and are generally present before the onset of sawtooth activity.

Strong Mirnov coil signals with low (m,n) were also obtained at frequencies <50 kHz: these resemble fishbone oscillations observed in conventional tokamaks.[13] The signals are of two types: fixed frequency bursts, lasting for up to 2–3 ms; and bursts which sweep down in frequency, over a longer timescale (up to about 1 ms) than the chirping modes described above (Fig. 13, 34–35 ms). Frequency-sweeping fishbones were often observed immediately before or during a sawtooth crash. Although there is no evidence of chirping modes or fishbones having a strong effect on plasma heating or confinement, such modes were weak or completely absent in high performance shots with $\beta_t > 30\%$.

Three distinct mechanisms have been proposed for fishbones observed in conventional tokamaks, all requiring $q_0 < 1$ and destabilization of the $m=1$ internal kink mode. One mechanism predicts a mode frequency correlated with the precessional drift frequency of trapped energetic ions;[31] the other two predict frequencies related to the thermal ion diamagnetic frequency (ω_i^*), with the kink mode being driven unstable by either trapped[14] or passing[32] energetic ions. Because tangential coinjection is used in START, only a small minority of beam ions are trapped and further the trapped beam ion population is weighted towards a region of velocity space lying close to the trapped/copassing boundary. At such pitch angles drift reversal occurs[33] and the precessional drift fishbone mode identified in Ref. 31 cannot be driven. Furthermore, since fishbone-like bursts had a frequency consistent with ω_i^*, it appears likely that such emission resulted from kink mode excitation by passing beam ions. However it is not yet clear why a high proportion of fishbone-like modes in START exhibited frequency sweeping.

B. Fixed-frequency modes in Alfvén frequency range

Fixed-frequency modes in START are observed less frequently than chirping modes, at relatively low NBI power and β_t, last for between 2 and 5 ms, and have frequencies in the range 50–350 kHz, which fits with the TAE gap frequency. The power spectrum of one such fixed-frequency set of modes is shown in Fig. 14. To study these fixed frequency Alfvén modes, the CSCAS code,[34] valid for tokamak plasmas of arbitrary aspect ratio, has been used to compute the struc-

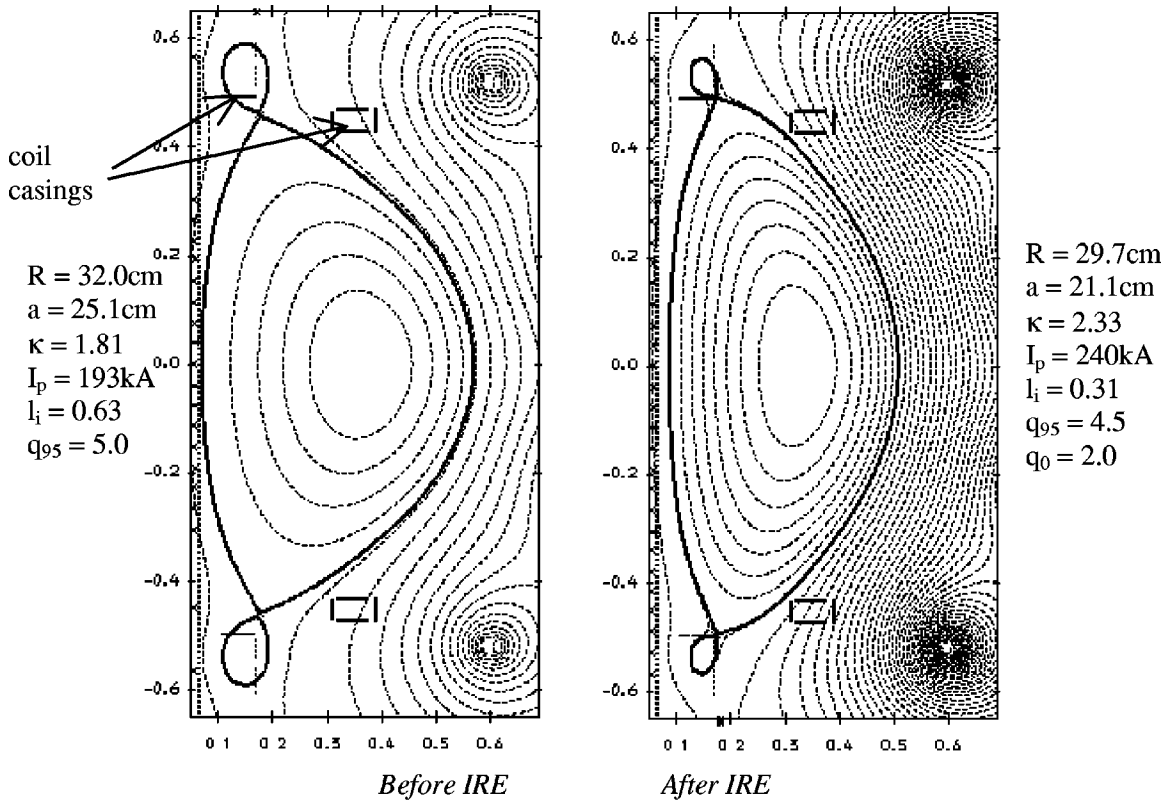

FIG. 12. Modeled pre-IRE and post-IRE states for a diverted START plasma. Note the strong elongation post-IRE.

ture of continuous MHD spectra in START. Equilibrium data corresponding to times of beam-driven instability were used. Experimentally the dominant modes in Fig. 14 are odd-n (probably $n=1$) but with a significant even-n (probably $n=2$) component. The continuum spectrum corresponding to a toroidal mode number $n=1$ is shown in Ref. 35 while the continuum spectrum for $n=2$ is shown in Fig. 15; both use reconstructed equilibria corresponding to the time of measurement of the power spectrum shown in Fig. 14. A key feature of Fig. 15 (and the $n=1$ spectra in Ref. 35) is the existence of wide gaps close to crossing points of the cylindrical shear Alfvén wave eigenfrequencies. The wide gaps can be qualitatively understood in terms of the theory of Fu and Van Dam.[36]

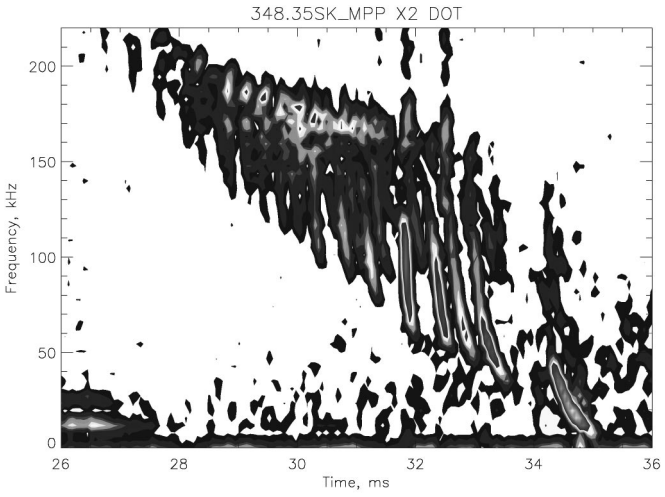

FIG. 13. Spectrogram from START shot 34835, showing a sequence of chirping modes at >50 kHz (28–34 ms) of increasing intensity and a more slowly chirping, fishbone-like mode at <50 kHz (34–35 ms). The toroidal β was 5%.

Discrete Alfvén eigenmodes (AEs) exist in the vicinity of each of the cylindrical crossing points noted above: any of these modes could, in principle, be driven unstable by energetic beam ions. We have used an ideal incompressible MHD code MISHKA-1[22] to compute toroidal Alfvén eigenfunctions for the lowest frequency gap in Fig. 15: the radial velocity $v_r(s)$ corresponding to one such eigenfunction is shown in Fig. 16. The first four frequency eigenvalues are 113, 124, 144, and 161 kHz in the plasma frame. The frequencies in the laboratory frame are shifted from those in the plasma frame by nv_ϕ where v_ϕ is the toroidal rotation frequency. This is measured to be peaked in the plasma center, a typical maximum value being about 15 kHz.

The fact that the computed $n=1$ (see Ref. 35) and $n=2$ frequencies are of the same order as those of the strongest peaks in Fig. 14, and exhibit multiple modes in the lowest frequency gap, suggests that the multiple TAE interpretation may be correct. It is also possible, however, that the series of peaks in Fig. 14 could have arisen from the excitation of either kinetic TAEs (associated with finite thermal ion Larmor radius effects) or low shear Alfvén eigenmodes.[37] Further analysis will be required to determine which type of mode best explains the observed fine structure.

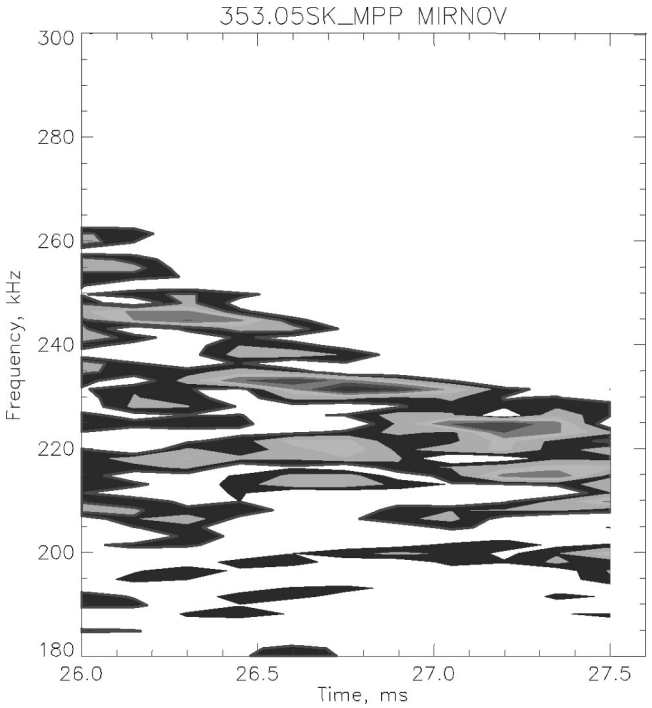

FIG. 14. Spectrogram from START shot 35305, showing a set of fixed frequency modes, with a frequency separation of about 14 kHz.

To understand the drive for fast particle modes in START the distribution function is required. An important property of the START NBI distribution[38] function was the existence of a steady-state bump-on-tail. The bump-on-tail arises because many beam ions traverse regions of high neutral density beyond the last closed flux surface, and, consequently, have a high probability of being neutralized. Since the neutralization probability increases as beam ions slow down, a bump-on-tail can result from the combined effects of Coulomb collisions and charge exchange. Thus, whereas in conventional tokamaks energetic ions provide free energy to drive AEs through pressure gradients alone,[36] in START a comparable drive is provided by beam ion distributions with $\partial f_b/\partial E>0$.

These results provide some optimism for future $D-T$ STs, since although a range of Alfvén instabilities have been observed in START, there is no evidence of them having a detrimental effect. Furthermore the bump-on-tail drive present in START will be absent in the next generations of larger size STs and on any ST technology device.

VII. SUMMARY

The ST obeys essentially the same operating limits as the conventional aspect ratio tokamak:
(i) The highest β is well described by a Troyon limit with $\beta_n \lesssim 5$, although it is not clear if this represents a MHD β limit or a confinement limit (i.e., whether more NBI power would raise β); (ii) the maximum accessible density is well defined by the Greenwald density $n_{\mathrm{GW}} \sim 1$ (with the exception of pellet fueled discharges); (iii) empirically the START normalized plasma current is limited so that $q_{95} \gtrsim 2$.
In the double null START configuration each of the above operating limits results in a current terminating disruption, though the current termination is relatively slow in the case of the density limit. Precursor MHD to these disruptions are not always observed, though the lack of outboard magnetic coils may mean that MHD with a strong in–out ballooning character is being missed. In the high β, but not high density, disruptions a clear energy quench phase precedes the current quench. Coherent MHD is observed during the high-β energy quench phase.

Theoretically there is scope to improve on both the attainable β and q_{95}. MHD stability calculations for START plasma geometry, including the full separatix, show it should be possible to double the normalized plasma current with a resulting increase in stable β, though a wall at 1.3 minor radii is needed for $n=1$ stability. At ultralow aspect ratio $(R/a=1.1)$ these high normalized current limit cases can

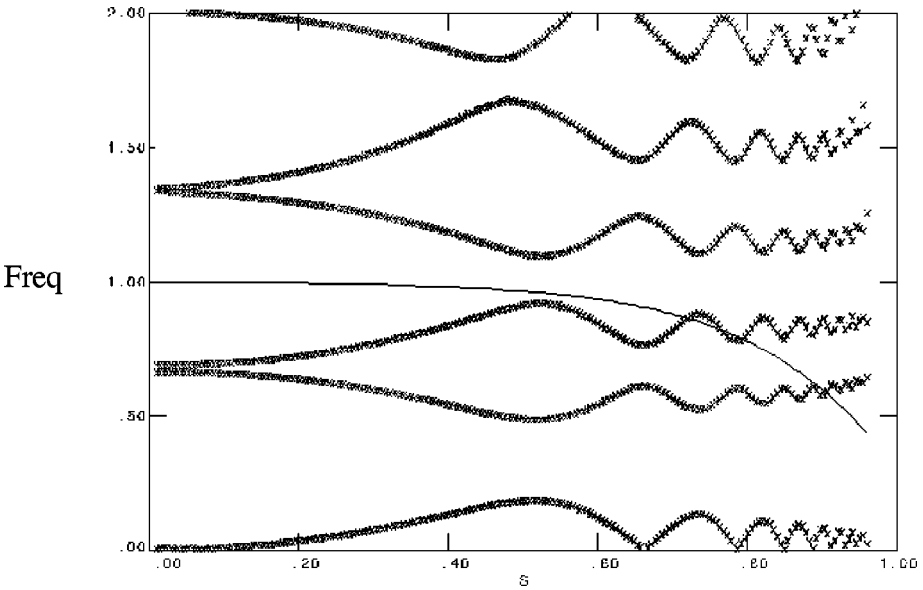

FIG. 15. Structure of ideal Alfvén continua for $n=2$ in START shot 35305. The radial variable is defined by s^2 being the normalized poloidal flux. Frequency is normalized by the axial Alfvén frequency $c_A(0)/R_0(=660\ \mathrm{kHz})$. The ''parabolic'' line shows the normalized electron density profile.

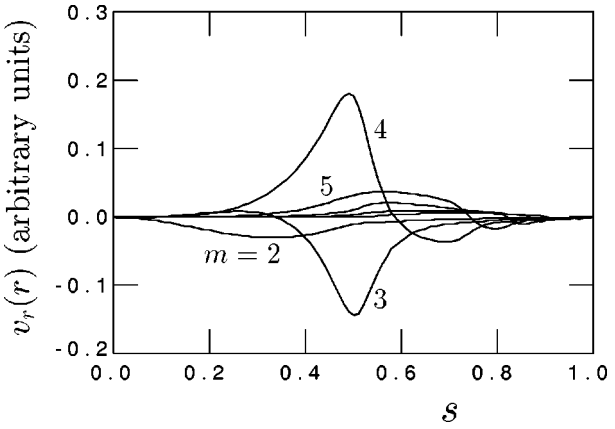

FIG. 16. Ideal-MHD radial velocity eigenfunction corresponding to the lowest-frequency gap in Fig. 15. Frequency eigenvalue in the plasma frame is 258 kHz.

have a stable $\beta_t > 100\%$ even without a conducting wall. The other route to increasing β is by tailoring the current profile to give second stable access for ballooning modes, which allows high $\beta_n(\sim 8)$, but again at the price of needing a wall at ~ 1.2 minor radii for low-n stability. These second stable cases can have high pressure driven current fractions $(I_{\nabla P}/I_p \gtrsim 90\%)$, unlike the high normalized current cases (where $I_{\nabla P}/I_p \sim 10\%$), making them well suited as the basis for electricity generating power plants.

Historically the disruption behavior in START has been found to depend on magnetic configuration—limiter or double null. Before the divertor coils were installed no rapid current terminating disruptions were observed in START (the only exception being pulses with rapid vertical field ramps in which the plasma is forced to interact strongly with the center column); instead IREs which have the main signatures of a disruption, except the I_p quench, occurred. After the divertor coils were installed strong interactions with them were observed as the plasma elongates at the I_p spike (negative loop voltage spike) and it is thought that this makes disruptions much more common in double null discharges. The main characteristics of the disruptions, or IREs, are quantitatively well explained by a model in which helicity is conserved during the event. Disruptions in double null discharges can trigger VDEs but it is found that the resulting halo currents flowing in the center column at ~ 15 cm above the X point are low; this result is promising but needs to be more fully explored in the next generation of STs.

The final topic addressed in this paper is the effect of the fast beam ions on MHD. Due to the low toroidal field the beam ions are naturally super-Alfvénic—making the ST well suited to studying TAE modes with the results transferable to conventional aspect ratio machines. NBI heated discharges do in general show MHD activity in the TAE frequency range, an exception being the highest-β pulses. The observed Alfvénic modes may either have a chirping character or at lower NBI power multiple frequency bands of modes may exist. Calculations show wide gaps in the Alfvén continuum for START equilibria and the existence of several unstable modes in each gap, possibly explaining the observation of several modes of different frequency coexisting. Lower frequency (<50 kHz) chirping modes are also observed and these are thought to be fishbone-like modes driven by passing beam ions. These results are promising for future technology applications of the ST, where α particles are expected to be super-Alfvénic and possibly drive TAEs, since despite a range of TAEs being observed in START there is no evidence for them having detrimental effects.

The results discussed in this paper provide a good basis and framework for studying MHD limits in the next generation of STs [such as the mega-amp spherical tokamak[39] (MAST) or the national spherical torus experiment[40] (NSTX)], which are just coming into operation. Beyond confirming the START results, there are promising routes for further improving operational limits and thus demonstrating the physics needed for an economic fusion power plant.

ACKNOWLEDGMENTS

This work is jointly funded by Euratom and the United Kingdom Department of Trade and Industry. The CRPP author was supported in part by the Swiss National Science Foundation. The NBI equipment on START is loaned by the U.S. Department of Energy, the Pellet Injector experiments were in collaboration with Risø and ENEA Frascati, and the EFIT reconstruction code is supplied by General Atomics. The MISHKA code was kindly provided by Dr. Huysmans, Dr. Sharapov, Dr. Kerner, and Dr. Mikhailovskii.

[1] Y.-K. M. Peng and D. J. Strickler, Nucl. Fusion **26**, 769 (1986).
[2] F. Troyon, R. Gruber, H. Saurenmann *et al.*, Plasma Phys. Controlled Fusion **26**, 1A209 (1984).
[3] J. A. Wesson and A. Sykes, Nucl. Fusion **25**, 85 (1985).
[4] A. Sykes, E. Del Bosco, R. J. Colchin *et al.*, Nucl. Fusion **32**, 694 (1992).
[5] M. Ono, C. B. Forrest, Y. S. Hwang *et al.*, *Proceedings 14th Conference on Plasma Physics and Controlled Fusion, Würzburg, 1992*, edited by J. Weil and M. Spak (International Atomic Energy Agency, Vienna, 1993), Vol. 1, p. 693.
[6] T. R. Jarboe, B. B. A. Nelson, A. K. Martin *et al.*, *Proceedings 15th Conference on Plasma Physics and Controlled Fusion, Seville, 1994*, edited by J. Weil and M. Spak (International Atomic Energy Agency, Vienna, 1995), Vol. 1, p. 725.
[7] G. D. Gartska, R. J. Fonck, and T. Intrator, Bull. Am. Phys. Soc. **41**, 1400 (1996).
[8] H. Toyama, K. Hanada, and K. Yamagashi, *Proceedings of the 24th EPS Conference on Controlled Fusion and Plasma Physics* (European Physics Society, Geneva, 1991), Vol. 21c, Part I, p. 417.
[9] A. Sykes, Phys. Plasmas **4**, 1665 (1997).
[10] D. A. Gates, R. Akers, L. Appel *et al.*, Phys. Plasmas **5**, 1775 (1998).
[11] A. Sykes, M. Bevir, R. A. Bamford *et al.*, *Proceedings 15th Conference on Plasma Physics and Controlled Fusion, Seville, 1994*, edited by J. Weil and M. Spak (International Atomic Energy Agency, Vienna, 1995), Vol. 1, p. 719.
[12] M. Greenwald, Nucl. Fusion **28**, 2199 (1988).
[13] K. McGuire, R. Goldston, M. Bell *et al.*, Phys. Rev. Lett. **50**, 891 (1983).
[14] B. Coppi, P. Detragiache, S. Migliuolo *et al.*, Phys. Rev. Lett. **63**, 2733 (1989).
[15] L. L. Lao, H. St. John, R. D. Stambaugh *et al.*, Nucl. Fusion **25**, 1611 (1985).
[16] A. Sykes, *Proceedings 17th Conference on Plasma Physics and Controlled Fusion, Yokohama, 1998* (International Atomic Energy Agency, Vienna, 1999), paper IAEA-CN-69/OV2/5.
[17] J. A. Wesson, R. D. Gill, D. J. Ward *et al.*, Nucl. Fusion **29**, 641 (1989).
[18] R. Yoshino, N. Fujisawa, J. Wesley *et al.*, *Proceedings of the 17th Conference on Plasma Physics and Controlled Fusion, Yokohama, 1998* (International Atomic Energy Agency, Vienna, 1999), paper IAEA-CN-69/ITERP1/14.

[19]L. Degtyarev, A. Martynov, S. Medvedev *et al.*, Comput. Phys. Commun. **103**, 10 (1997).
[20]T. C. Hender, A. Bond, J. Edwards *et al.*, ''Spherical Tokamak Power Plant Design Issues,'' Fus. Eng. Design (submitted).
[21]E. J. Strait, M. S. Chu, J. R. Ferron *et al.*, *Proceedings of the 18th EPS Conference on Controlled Fusion and Plasma Physics* (European Physics Society, Geneva, 1991), Vol. 15c, Part II, p. 105.
[22]A. B. Mikhailovskii, G. T. A. Huysmans, W. O. K. Kerner *et al.*, Plasma Phys. Rep. **23**, 844 (1997).
[23]R. L. Miller, Y. R. Lin Liu, A. D. Turnbull *et al.*, Phys. Plasmas **4**, 1062 (1997).
[24]J. E. Menard, S. C. Jardin, S. M. Kaye *et al.*, Nucl. Fusion **37**, 595 (1997).
[25]S. G. Bespoludennov, L. M. Degtyarev, and S. Y. Medvedev, Sov. J. Plasma Phys. **12**, 441 (1986).
[26]C. Ribeiro, M. J. Walsh, G. F. Counsell *et al.*, *Proceedings of the 25th EPS Conference on Controlled Fusion and Plasma Physics* (European Physics Society, Geneva, 1998), Vol. 22c, p. 842.
[27]M. R. O'Brien, R. J. Akers, R. A. Bamford *et al.*, *Proceedings of the 16th Conference on Plasma Physics and Controlled Fusion, Montreal, 1996*, edited by J. Weil and M. Spak (International Atomic Energy Agency, Vienna, 1997), Vol. 12, p. 57.
[28]M. Ono, D. Stutman, Y. S. Hwang *et al.*, *Proceedings of the 16th Conference on Plasma Physics and Controlled Fusion, Montreal, 1996*, edited by J. Weil and M. Spak (International Atomic Energy Agency, Vienna, 1997), Vol. 12, p. 71.
[29]A. Sykes, Plasma Phys. Controlled Fusion **36**, B93 (1994).
[30]W. W. Heidbrink, Plasma Phys. Controlled Fusion **37**, 937 (1995).
[31]L. Chen, R. B. White, M. N. Rosenbluth *et al.*, Phys. Rev. Lett. **52**, 1122 (1984).
[32]J. Betti and J. Freidberg, Phys. Rev. Lett. **70**, 3428 (1993).
[33]C. M. Roach, J. W. Connor, and S. Janjua, Plasma Phys. Controlled Fusion **37**, 679 (1995).
[34]S. Poedts and E. Schwartz, J. Comput. Phys. **105**, 165 (1993).
[35]K. G. McClements, M. P. Gryanevich, S. E. Sharapov *et al.*, ''Physics of Energetic Particle-Driven Instabilities in the START Spherical Tokamak,'' Plasma Phys. Controlled Fusion (accepted).
[36]G. Y. Fu and J. W. Van Dam, Phys. Fluids B **1**, 1949 (1989).
[37]J. Candy, B. N. Breizmann, J. W. Van Dam *et al.*, Phys. Lett. A **215**, 299 (1996).
[38]R. J. Akers *et al.*, in Controlled Fusion and Plasma Physics (Proceedings 25th EPS Conference on Controlled Fusion and Plasma Physics (European Physics Society, Geneva, 1998), paper G81.
[39]A. C. Darke *et al.*, ''MAST: A mega amp spherical tokamak,'' Fusion Technol. **1**, 799 (1995).
[40]C. Neumeyer *et al.*, ''Engineering Overview of the National Spherical Torus Experiment (NSTX),'' *Proceedings of the 17th IEEE/NPSS Symposium on Fusion Engineering, San Diego* (Institute of Electrical and Electronics Engineers, Piscataway, NJ, 1997).